

Article

Enhanced Phosphate Removal by Hydrated Lanthanum Oxide-Modified Quaternized Polyaniline Nanocomposite: Performance and Mechanism

Enhui Ji ¹ , Minglong Fang ² and Haixia Wu ^{1,*} ¹ College of Urban Construction, Nanjing Tech University, Nanjing 211800, China; 202361224015@njtech.edu.cn² Architectural Design and Research Institute Co., Ltd., Nanjing Tech University, Nanjing 210009, China; 2022L0001934@njtech.edu.cn

* Correspondence: wuhaixia@njtech.edu.cn

Abstract: Phosphorus mainly exists in the form of phosphate in water. Excessive phosphorus can cause eutrophication, leading to algae reproduction and the depletion of oxygen in water, destroying aquatic ecology. This study prepared quaternized polyaniline (PN) and quaternized polyaniline with lanthanum hydrate (HLO-PN), and a new nanocomposite for removing phosphate from wastewater was proposed. The results of adsorption experiments show that HLO-PN can effectively remove phosphate in the range of pH 3–7; the maximum adsorption capacity is 92.57 mg/g, and it has excellent anti-interference ability against some common coexisting anions (F^- , Cl^- , NO_3^- , SO_4^{2-}) other than CO_3^{2-} . After five adsorption–desorption cycles, the phosphate adsorption capacity (60 mg/g) was still 74.28% of the initial adsorption capacity (80.85 mg/g), indicating that the HLO-PN nanocomposites had good reusability and recovery of phosphorus. The characterization results show that phosphate adsorption is realized by electrostatic adsorption and ligand exchange.

Keywords: phosphate; adsorption; quaternized polyaniline; lanthanum



Citation: Ji, E.; Fang, M.; Wu, H. Enhanced Phosphate Removal by Hydrated Lanthanum Oxide-Modified Quaternized Polyaniline Nanocomposite: Performance and Mechanism. *Sustain. Chem.* **2024**, *5*, 258–272. <https://doi.org/10.3390/suschem5040017>

Academic Editor: Matthew Jones

Received: 4 September 2024

Revised: 28 October 2024

Accepted: 29 October 2024

Published: 31 October 2024



Copyright: © 2024 by the authors. Licensee MDPI, Basel, Switzerland. This article is an open access article distributed under the terms and conditions of the Creative Commons Attribution (CC BY) license (<https://creativecommons.org/licenses/by/4.0/>).

1. Introduction

In today's world, pollution of water resources has become an increasingly serious problem, especially the excessive discharge of phosphate, which not only threatens the ecological balance of water bodies but also may lead to environmental issues such as water blooms. Therefore, the development of efficient and sustainable phosphate removal technologies is an important issue in the field of environmental science [1,2]. China's "Pollutant Emission Standards for Urban Wastewater Treatment Plants" (GB18918-2002) stipulates special pollution limits for total phosphorus in different levels of wastewater treatment plants, and the standards for Class I A and B are 0.5 and 1.0 mg/L, respectively. The United States Environmental Protection Agency (USEPA) stipulates that the maximum phosphate concentration in a river entering a lake or reservoir should be less than 0.05 mg/L [3]. Various methods (e.g., chemical precipitation, biological, and ion exchange) have been used to remove phosphate pollution for decades. Unfortunately, these processes have various limitations such as high treatment costs and energy consumption, which limit their effectiveness in removing phosphate from water [1]. In contrast, adsorption has great potential due to its cost-effectiveness and simplicity of operation [2–4].

Many adsorbents have been developed for phosphate removal in previous studies. The main active ingredients are La, Mn, Al, Fe and Zr [5–8]. Metal (hydrogen) oxides, such as Fe(III), Al(III) and La(III) nanoparticles, are effective materials for phosphate removal [9–12]. These metal (hydrogen) oxides exhibit a good affinity for phosphate through inner-sphere complexation [13] including aluminum oxide [14], hydrated iron oxides (HFOs) [15], hydrated zirconium oxides (HFOs) [16], lanthanum (hydrated) oxides [17], etc. Among these transition metals, lanthanum (La) is an environmentally friendly rare earth element

found in abundance in the earth's crust and readily forms stable La^{3+} ions. With its Lewis acid nature, La has a high ligand adsorption capacity for phosphates even at low concentration levels [18]. Due to the strong affinity of lanthanum for phosphate, many studies have produced La-modified adsorbents such as La-modified bentonite (Phoslock), and La-doped silica [19]. However, Phoslock has a maximum adsorption capacity of only 9.6 to 10.5 mg P/g [19], exhibiting a slightly enhanced phosphate adsorption capacity. In addition, the large-scale application of these adsorbents is limited by fine particle morphology, poor mechanical strength and potential release. To overcome these problems, increasing attention has been paid to lanthanide-based composites by confining the active metal (hydrogen) oxides within a polymer body [20]. Such composites combine the specific affinity of lanthanum (water) oxides for phosphates with the excellent mechanical properties of the host material [13], both preventing metal ion leakage and dispersing the active sites.

Polyaniline is one of the polymeric compounds with a big surface area and an easy synthesis method. However, the native polyaniline molecular structure lacks specific functional groups for adsorption reactions with phosphates. By introducing a large number of quaternary ammonium groups immobilized on the polyaniline molecule, the surface of polyaniline is positively charged, which can form an electrostatic interaction with negatively charged phosphate and enhance the adsorption effect [21]. Consequently, a promising method for eliminating low phosphate concentrations is the coupling of nano-La(III) (hydro)oxides with polyaniline modified by quaternary amines.

In this study, a lanthanide-based nanocomposite, HLO-PN, was synthesized by in situ nucleation of hydrated lanthanum oxide (HLO) nanoparticles within a quaternized polyaniline (PN) backbone. A detailed investigation was conducted into the characteristics of the nanocomposites. The removal effect of PN and HLO-PN on phosphate under specific conditions was investigated to determine the optimal dosage and acid–base environment. Adsorption kinetics, adsorption isotherms and thermodynamic studies were carried out. Kinetic data were fitted to quasi-primary, quasi-secondary and intraparticle diffusion models. Isotherm data were fitted to Langmuir, Freundlich, Temkin and D-R models. The effect of coexisting ions on the adsorption of phosphate by the material is investigated. In addition, the reusability of functionalized adsorbents is investigated and possible adsorption mechanisms are explored in depth.

2. Materials and Methods

2.1. Materials

All the chemicals were of analytical grade and did not require further purification. Polyaniline was purchased from Shanghai McLean Biochemical Technology Co., Ltd. (Shanghai, China), dichloroethane was purchased from Shanghai Titan Technology Co., Ltd. (Shanghai, China), chloromethyl ether was purchased from Shanghai Myriad Biochemical Technology Co., Ltd. (Shanghai, China), zinc chloride was purchased from Jiangsu Jiuding Biotech Co., Ltd. (Rugao, China), and trimethylamine solution and lanthanum chloride heptahydrate were purchased from Shanghai Aladdin Biochemical Technology Co., Ltd. (Shanghai, China). The water used in the test was pure water produced by the EPCE water system.

2.2. Methods

2.2.1. Synthesis of PN

In the preparation process of quaternized polyaniline (PN), 20 g of polyaniline (PS) was added to 200 mL of dichloroethane solution, swelled for 24 h, filtered, and dried at 373 K. The dried particles were transferred to a pressure flask containing 200 mL of chloromethyl ether; 20 g of anhydrous zinc chloride was added, and the mixture was continuously stirred at 220 rpm for 12 h at 313 K and filtered. The filtered particles were added to a 200 mL pressure flask containing 30% trimethylamine solution and reacted at 318 K for 24 h. Finally, the quaternized polyaniline was obtained by washing with 200 mL ethanol and 2000 mL pure water and drying at 333 K for 6 h.

2.2.2. Synthesis of HLO-PN

Hydrated metal oxides were loaded onto PN by precursor impregnation diffusion and in situ co-precipitation; 17.6 g $\text{LaCl}_3 \cdot 7\text{H}_2\text{O}$ and 15 g PN were added to a pressure flask containing 1 mL HCl and 120 mL ethanol and continuously stirred at 333 K for 8 h before filtration and drying. The dried particles were added to 1000 mL of 5% NaOH solution and constantly stirred at 298 K for 10 h before filtration. Finally, the mixture was washed with 200 mL ethanol and 2000 mL pure water and dried at 333 K for 6 h.

2.2.3. Batch Experiments

Potassium dihydrogen phosphate (KH_2PO_4) was dissolved in pure water to prepare a reserve solution with a phosphate concentration of 1000 mg/L, which was refrigerated in a brown bottle. When used, a phosphate solution with a concentration of 10 mg/L was obtained by diluting the reserve solution. The adsorbent and phosphate solution were added into 60 mL or 250 mL pp plastic bottles, sealed and placed in a water-bath oscillator to carry out the adsorption reaction at 200 rpm; the reaction time was determined according to the requirements of the test, and at the end of the reaction, the supernatant was taken with a syringe and then filtered through a disposable filter with a pore size of 0.45 μm . With pure water as the blank control, the absorbance of the filtrate was measured by an ultraviolet-visible spectrophotometer (UV-5500 Shimadzu Co., Ltd., Kyoto, Japan). The standard curve of phosphate was established according to the test data, and the concentration of phosphate in the filtrate was calculated. Each set of adsorption tests was performed three times and the results were averaged. Unless otherwise noted, the reaction temperature was 298 K, and the water bath shaker was preheated to ensure the stability of the test temperature. The initial pH of phosphate was adjusted by 0.1 M sodium hydroxide solution or 0.1 M hydrochloric acid. The adsorption kinetics test was conducted using 250 mL pp plastic bottles, whereas the other tests were conducted using 60 mL pp plastic bottles.

The adsorption process of phosphate by quaternized groups and hydrated metal oxides is generally reversible. The reversible effect is affected by the type and amount of eluent, and the amount of eluent has a greater impact on the reversible process [21]. The alkaline environment in the solution is conducive to the reversible process. In this study, NaOH solution was used as eluent. The material after adsorption of phosphate was treated with different concentrations of NaOH solution to observe the desorption efficiency of phosphate and evaluate the regeneration performance of the material. In order to study the reusability of the material, the desorbed solution was subjected to suction filtration. The desorbed material was washed with anhydrous ethanol and pure water, centrifuged and dried. The next adsorption test was performed using the optimal concentration of NaOH solution and repeated five times. It should be noted that the volume of eluent used in the desorption test is consistent with the volume of phosphate solution used in the adsorption test; the optimum concentration of NaOH solution was selected by considering the desorption efficiency and readsorption capacity of phosphate. The other conditions of the desorption test are consistent with the adsorption test, which is not explained here. For the formula of adsorption kinetics, the adsorption isotherm, and the adsorption thermodynamics, refer to the Supplementary Materials.

2.2.4. Characterization and Analysis

Ammonium molybdate and silver chloride spectrophotometric methods were used to detect phosphate and chloride concentrations in solution, respectively. A scanning electron microscope (Regulus8230, Hitachi, Kyoto, Japan) was used to observe the micro-morphology of the materials, and the elements of the materials were analyzed in combination with energy-dispersive spectroscopy (EDS). The specific surface area and pore structure of the materials were analyzed using a specific surface area analyzer (3flex, Micromeritics, Norcross, GA, USA). The crystal structure of the materials was examined using an X-ray diffractometer (D8 Advance, Bruker, Billerica, MA, USA). The zeta potential of the materials before and after phosphate adsorption was detected by a nanoparticle size

potential analyzer (Zetasizer Nano ZS90, Malvern Instruments, Malvern, UK). An infrared spectrometer (Nicolet iS20, Thermo Scientific, Waltham, MA, USA) was used to detect the chemical bonds and functional groups before and after the adsorption of phosphate on the materials. X-ray photoelectron spectroscopy (K-Alpha, Thermo Scientific, Waltham, MA, USA) was used to detect the chemical state of the elements before and after the adsorption reaction on the materials.

3. Results and Discussion

3.1. Characterization of HLO-PN

Scanning electron microscopy was used to analyze the morphology of PS, PN and HLO-PN. As shown in Figure 1a, a uniform surface particle (400 nm in diameter) structure can be observed in the morphology of PS, but after the quaternization process, the original surface particle structure is destroyed, and the surface morphology of PN is smoother (Figure 1b). HLO-PN shows a reticulated structure after LaOOH loading (Figure 1c). The primary components of PN, C (Figure 1d), N (Figure 1e), and Cl (Figure 1f), were present in the EDS mapping results of HLO-PN, indicating that La (Figure 1g) was uniformly distributed on PN and verifying the successful synthesis of HLO-PN.

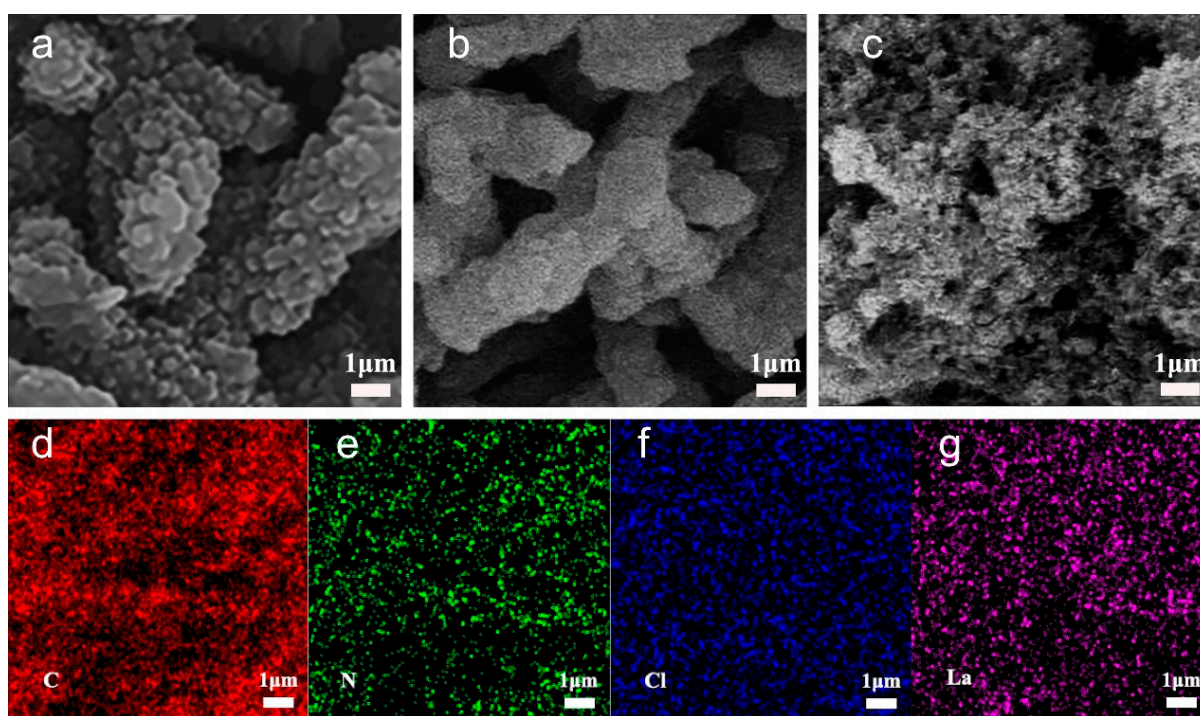


Figure 1. SEM images of (a) PS, (b) PN and (c) HLO-PN; EDS mapping of (d) carbon, (e) nitrogen, (f) chlorine and (g) lanthanum for HLO-PN.

As shown in Figure 2, the results of the pore distribution of (a) PN and (b) HLO-PN show that it mainly consists of mesopores and macropores, and the results of the N_2 adsorption-desorption experiments show a type II BET adsorption isotherm for unrestricted monolayer-multilayer adsorption [22]. As shown in Table S1, the specific surface area (BET) of PN was identified as $21.55 \text{ m}^2/\text{g}$, and the specific surface area of HLO-PN rose to $40.58 \text{ m}^2/\text{g}$ after LaOOH loading, indicating that LaOOH was successfully loaded onto PN.

As shown in Figure 2e,f, the 1599 cm^{-1} peak corresponds to the absorption vibration of the quinone structure $N=Q=N$ in polyaniline, the 1494 cm^{-1} peak represents the characteristic absorption vibration of the benzene structure $N-B-N$ in polyaniline, the 1375 cm^{-1} peak is due to the absorption of the C-N in the aromatic amine $Ar-N$, and the 1108 cm^{-1} peak represents the characteristic absorption vibration of the imide nitrogen structure $B-N=Q$ in polyaniline. The appearance of the above peaks indicates that there is a complete

polyaniline structure in both PN (Figure 2e) and HLO-PN (Figure 2f) [23,24]. The 1070 cm^{-1} peak corresponds to the C-N stretching vibration in N-alkyl, indicating the successful quaternization of polyaniline [25]. The 3411 cm^{-1} peak corresponds to the stretching vibration of -OH [26]. Notably, the 3411 cm^{-1} peak was observed in PN (Figure 2e), indicating that the chloride ion on PN was partially replaced by a hydroxyl group (Figure 2c). In addition, the peak at 636 cm^{-1} of HLO-PN is associated with the La-O lattice vibration of LaOOH, indicating that LaOOH (Figure 2d) was successfully loaded onto PN [27].

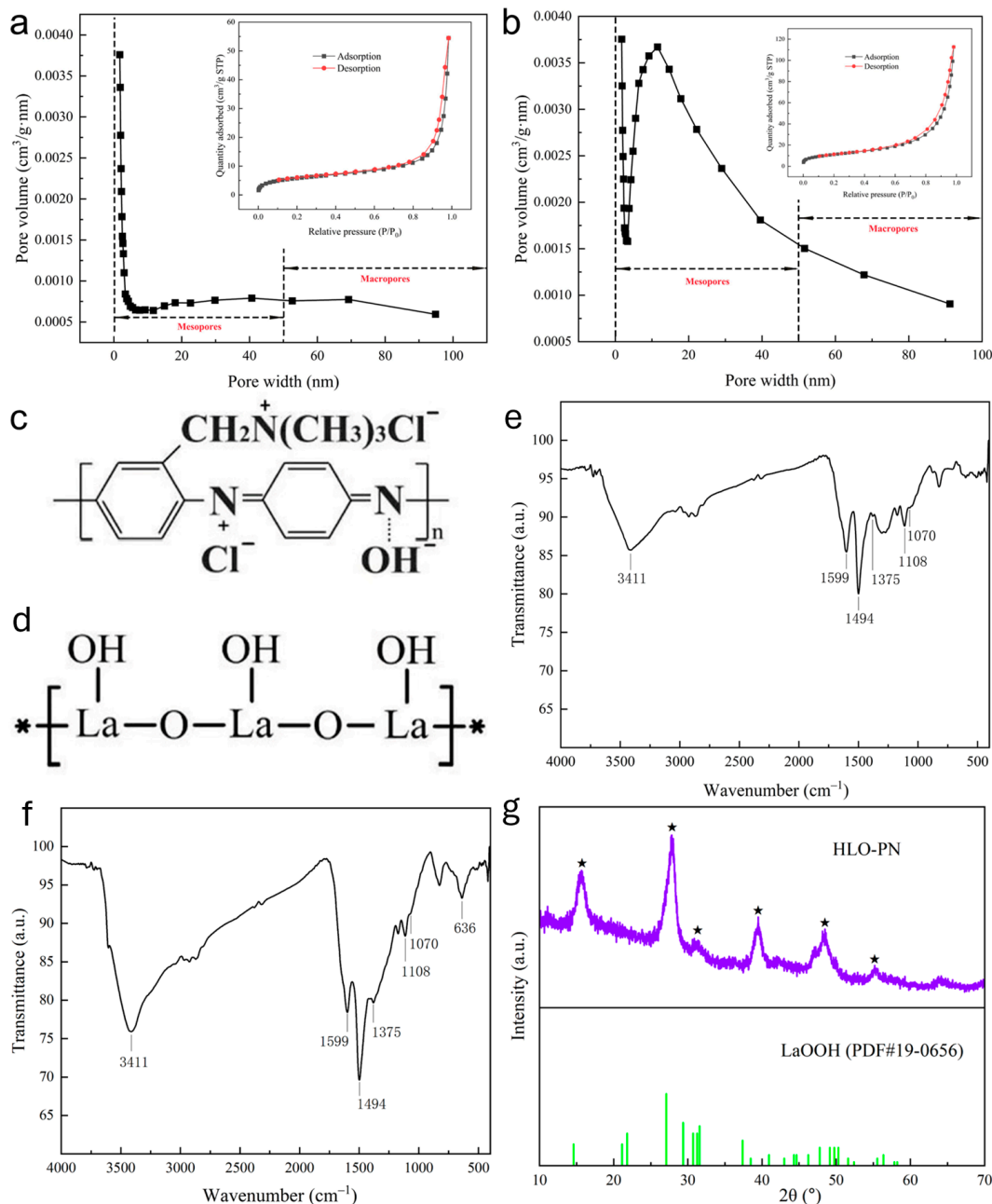


Figure 2. Pore diameter distributions and corresponding N_2 adsorption–desorption isotherms (inset) of (a) PN and (b) HLO-PN; structural formula for (c) PN and (d) LaOOH; FTIR spectra of (e) PN and (f) HLO-PN; XRD patterns of (g) HLO-PN. (*: Hydrated Lanthanum Oxide).

The XRD spectrum of HLO-PN is shown in Figure 2g. The labeled diffraction peaks match with PDF#19-0656 representing LaOOH, indicating that LaOOH was successfully loaded on PN.

3.2. Factors Affecting the Adsorption of Phosphate by HLO-PN

3.2.1. Effect of Dosage Rate

The effects of PS, PN and HLO-PN dosages (0.5–5.0 g/L) on phosphate removal were investigated at an initial solution pH of 5, 10 mg/L phosphate, a temperature of 298 K, and a contact time of 24 h. As shown in Figure S1a, the maximum phosphate removal was only 5.2% (4.0 g/L), indicating that the N⁺ activity in the quinone structure N=Q=N, the benzene structure N-B-N, and the imine nitrogen structure B-N=Q on PS is very low, which is similar to the previous report [28]. Subsequent phosphate adsorption tests were no longer considered for comparison tests with PS. As shown in Figure S1b, phosphate removal increased from 49.5% to 99.8% when PN dosing was varied in the range of 0.5–4.0 g/L. The removal rate remained stable (99.8%) by further increasing the PN dosage. The optimum PN dosage was determined to be 4.0 g/L, and all PN adsorption tests described after this subsection were conducted at this dosage. As shown in Figure S1c, phosphate removal increased rapidly from 61.3% to 99.8% when the HLO-PN dosage was varied in the range of 0.5–1.5 g/L. The removal rate remained stable (99.8%) by further increasing the dosage of HLO-PN. The optimum dosage of HLO-PN was determined to be 1.5 g/L, and all HLO-PN adsorption tests after this study were conducted at this dosage.

3.2.2. Effect of Solution pH

The pH dependence of phosphate adsorption by PN and HLO-PN was studied in the pH range of 1–12. Detailed experimental conditions: The initial phosphorus concentration was 10 mg/L, the initial pH was 5.8, and the reaction was adjusted by using 0.1 M HCl and 0.1 M NaOH solutions at 298 K for 24 h, with the dosages of PN and HLO-PN being 4 g/L and 1.5 g/L, respectively. As shown in Figure 3a, the removal efficiency of phosphate by PN firstly increased from 10.1% to 99.8% and then decreased to 15.7%. The highest removal rate was observed at pH 4. As shown in Figure 3b, the removal rate of phosphate by HLO-PN increased from 31.2% to 99.8% and then decreased to 8.7% in the range of pH 3.0–12.0, and showed an excellent removal rate (>83.3%) in the range of pH 3.0–5.0. The highest removal rate was observed at pH 5. Excellent removal (>80.2%) was shown in the pH range of 3.0–7.0. The gradual increase in the pH of the final solution after the adsorption of phosphate indicates that the application of HLO-PN adsorption of phosphate improves the alkalinity of the solution and helps to solve the problem of acidity in water.

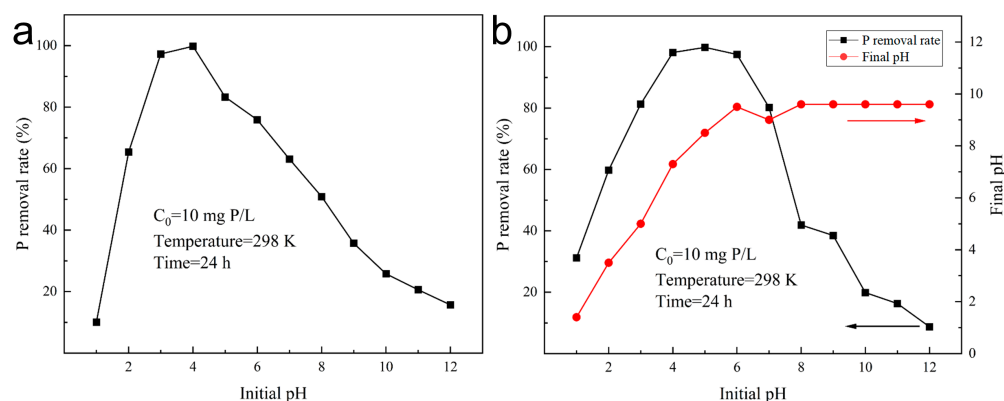


Figure 3. Effect of initial pH of solution on phosphate removal by (a) PN and (b) HLO-PN. (A red arrow indicates that the red curve is referenced to the right coordinate and a black arrow indicates that the black curve is referenced to the left coordinate).

3.2.3. Effect of Time

To explore the adsorption behavior of PN and HLO-PN on phosphate, phosphate removal kinetic studies were carried out. As shown in Figure 4a, the phosphate removal by adsorption increased dramatically in the first 1 h. The adsorption of PN and HLO-PN was 79.07% and 83.13% of the final adsorption, respectively. Over time, the adsorbent became

saturated and the number of active sites decreased. The adsorption capacity of PN and HLO-PN increased slowly and tended to be balanced at about 6 h. The adsorption capacity of PN and HLO-PN was 93.02% and 92.77% of the final adsorption capacity, respectively. To quantitatively describe the adsorption of phosphate on PN and HLO-PN, kinetic data were fitted using three well-known kinetic models, quasi-primary, quasi-secondary and intraparticle diffusion models. As shown in Table S2, the quasi-secondary kinetic model fitted the experimental data with high R^2 values (0.9902 for PN and 0.9962 for HLO-PN), indicating the chemisorption characteristics of phosphate on PN and HLO-PN. It is noteworthy that the quasi-secondary kinetic constant K_2 (0.067) for HLO-PN is larger than that of K_2 (0.054) for PN, indicating that the adsorption rate of phosphate by HLO-PN is faster than that of PN [29].

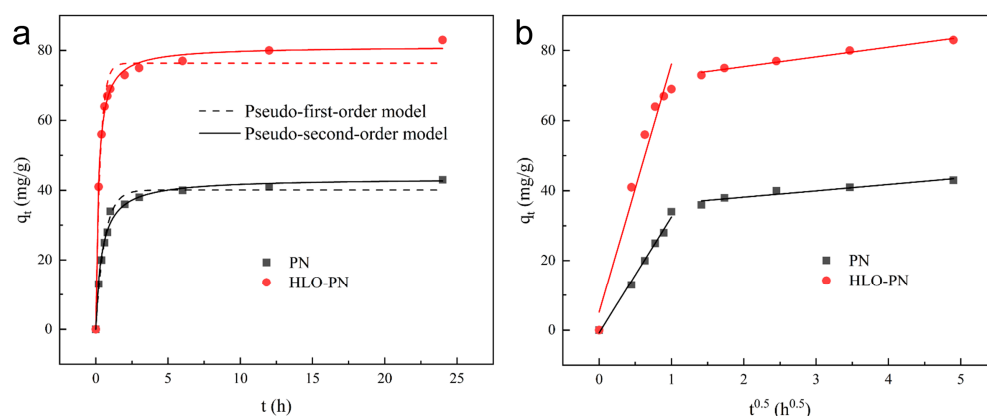


Figure 4. (a) Fitting of pseudo-first-order and pseudo-second-order kinetic models of phosphate by PN and HLO-PN. (b) Fitting of PN and HLO-PN to the phosphate in-particle diffusion model ($C_0 = 200$ mg/L, pH 5.0, PN dosage 4.0 g/L, HLO-PN dosage 1.5 g/L, temperature 25 °C).

The fitted straight lines showed good R^2 values and deviated from the origin, according to the intraparticle diffusion modeling results (Figure 4b and Table S3), suggesting that the adsorption of phosphate on PN and HLO-PN involves an intraparticle diffusion process. In addition, the simulation results for phosphate adsorption showed a twofold linearity, implying that two coexisting adsorption mechanisms (surface adsorption and intraparticle diffusion) are involved in the adsorption of phosphate on PN and HLO-PN [30].

3.2.4. Effect of Temperature

To further describe the interaction between phosphate and adsorbents, adsorption isotherm tests were performed. The adsorption of phosphate by PN (Figure 5a) and HLO-PN (Figure 5b) gradually increased with the increase in the initial concentration (10–500 mg/L) until equilibrium was reached. This is because a higher concentration gradient enhances the adsorption driving effect in the initial stage, but also stimulates the competition between adsorbents for the limited adsorption sites [31]. In addition, the adsorption of phosphate showed an increasing trend as the water temperature increased from 15 °C to 35 °C, indicating the heat-absorbing nature of phosphate adsorption on PN and HLO-PN. Langmuir, Freundlich, Temkin and D-R isotherm models were used to study the interaction between PN and HLO-PN and phosphate, as shown in Figure 5a–d. Based on the R^2 values of the models (Tables S4 and S5), it can be seen that the applicability of the above four models for phosphate adsorption on PN and HLO-PN is in the order of Langmuir > Temkin > Freundlich > D-R. The experimental data are most consistent with the Langmuir isotherm model, which suggests that the adsorption of phosphate by PN and HLO-PN is related to the monolayer adsorption process. Notably, the Langmuir parameter K_L for phosphate adsorption by PN and HLO-PN increases with increasing temperature, indicating that the adsorption between PN and HLO-PN and phosphate is relatively stronger at higher temperatures [32]. This is because rising temperatures

increase the amount of available active sites on the adsorbent's surface and give phosphate molecules more energy to move, which facilitates their interaction with the surface of the adsorbent [33]. Based on the Langmuir model, the maximum adsorption capacities of PN and HLO-PN were calculated to be 54.05 and 92.57 mg/g, respectively. The binding energy involved in the physisorption process is reported to be less than 1 kJ/mol, corresponding to the parameter b in the Temkin isotherm model [34,35]. The D-R isotherm model uses the mean adsorption free energy (E) to determine the adsorption mechanism. The adsorption process was 8–16 kJ/mol for ion exchange and less than 8 kJ/mol for physical adsorption. The E values for PN and HLO-PN were in the range of 3.5–5.5 kJ/mol, which is close to 8 kJ/mol, suggesting that there is physical adsorption during the process, which may involve ion exchange [36]. Due to the non-specific adsorption (electrostatic attraction) of quaternary amine groups to phosphate and the specific adsorption (La–phosphate complexes) of lanthanum-containing groups to phosphate, the adsorption capacity of HLO-PN to phosphate is higher than that of previously reported hydrated lanthanum oxide-modified adsorbents (Table 1).

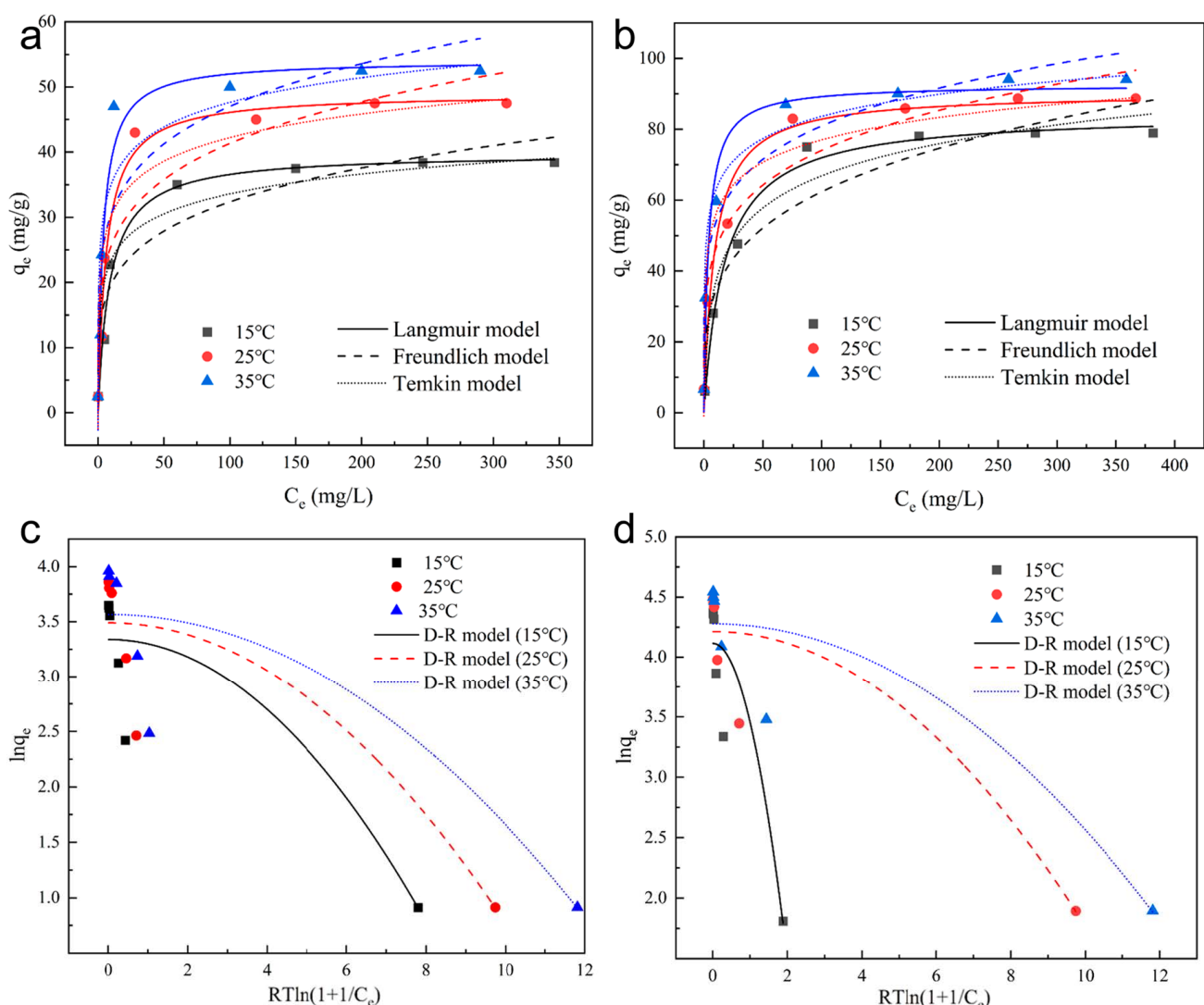


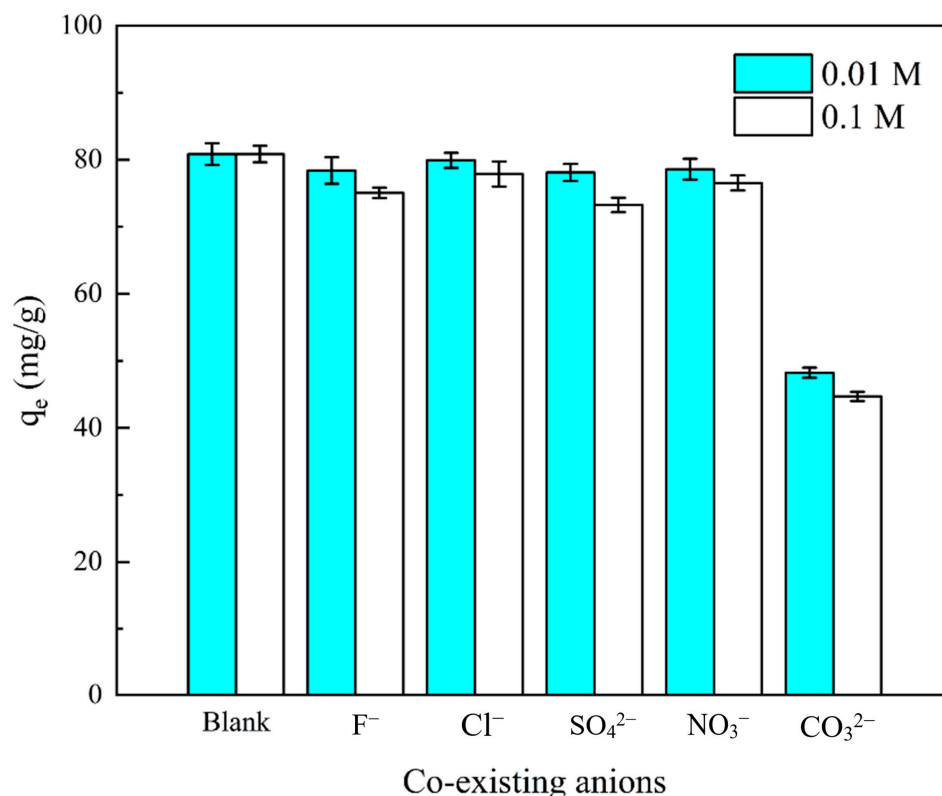
Figure 5. (a) PN's fitting of Langmuir, Freundlich and Temkin isotopes. Freundlich and Temkin isotherm models for phosphate; (b) HLO-PN's fitting of Langmuir, Freundlich and Temkin isotherm models for phosphate; (c) PN's fitting of D-R isotherm models for phosphate; (d) HLO-PN's fitting of D-R isotherm models for phosphate ($C_0 = 10$ –500 mg/L, pH 5.0, PN dosage 4.0 g/L, HLO-PN dosage 1.5 g/L, contact time 24 h).

Table 1. Comparison of various hydrated lanthanum oxide-modified adsorbents for phosphate adsorption.

Adsorbents	Isotherm	Adsorption Conditions		Phosphate Uptake q_{\max} (mg/g)	Ref.
		pH	T (°C)		
M-La(OH) ₃	Langmuir	7.0	25	52.7	[37]
La-CA-30	Langmuir	3.0	25	55.72	[38]
La-diatomite	Langmuir	5.6	25	58.7	[39]
La-ZFA	Langmuir	NA	25	71.94	[40]
La@CS	Freundlich	NA	30	76.6	[41]
La ₅ EV	Langmuir	5.0	25	79.6	[42]
HLO-PN	Langmuir	5.0	25	90.28	This work

3.2.5. Effect of Coexisting Ions

Figure 6 shows the effect of the coexisting anions F^- , Cl^- , NO_3^- , SO_4^{2-} and CO_3^{2-} on the phosphate adsorption capacity of HLO-PN. The phosphate adsorption capacity (q_e) of HLO-PN was 80.85 mg/g without any addition of competing anions. When the coexisting anion concentration of F^- , Cl^- , NO_3^- and SO_4^{2-} was 0.01 M, HLO-PN's q_e was barely impacted, suggesting that it has a strong ability to selectively adsorb phosphate anions. When the coexisting anion concentration of F^- , Cl^- , NO_3^- and SO_4^{2-} increased to 0.10 M, the q_e only slightly decreased, indicating that this competing anion hardly interferes with the strong adsorption of phosphate on HLO-PN in the presence of higher concentrations. In the presence of 0.01 and 0.1 M CO_3^{2-} , the adsorption capacity of phosphate on HLO-PN was 48.23 and 44.71 mg/g, which decreased by 40.35% and 44.70%, respectively. This is because the K_{sp} value of $La_2(CO_3)_3$ (3.98×10^{-34}) is smaller than that of $LaPO_4$ (3.7×10^{-23}) [43], which is favorable for phosphate adsorption on HLO-PN via CO_3^{2-} displacement, and the formed $LaPO_4$ was subsequently converted to $La_2(CO_3)_3$, thus reducing the phosphate adsorption capacity.

**Figure 6.** Effect of coexisting anions and their concentrations on the phosphate adsorption capacity by using HLO-PN ($C_0 = 200$ mg/L, pH 5.0, dosage 1.5 g/L, temperature 25 °C).

3.3. Adsorption Mechanism

3.3.1. Impact Analysis of pH

The ambient pH of the adsorption process is important as it affects not only the phosphate species but also the surface properties of the adsorbent. At different pH values, phosphate's morphology changes, which affects the efficiency of its adsorption by the adsorbent [44]. As shown in Figure 7a, when the solution pH is less than 2.12, phosphate exists mostly in the form of H_3PO_4 ; when it is between 2.12 and 7.21, it exists mostly in the form of H_2PO_4^- ; when the pH is between 7.21 and 12.31, it exists mostly in the form of HPO_4^{2-} ; when greater than 12.31, it is mostly in the form of PO_4^{3-} . As shown in Figure 7b, the zero-point potential of HLO-PN (5.27) after the adsorption of phosphate changes to 4.18, indicating that the adsorption of phosphate leads to the dissociation of surface hydroxyl groups [42].

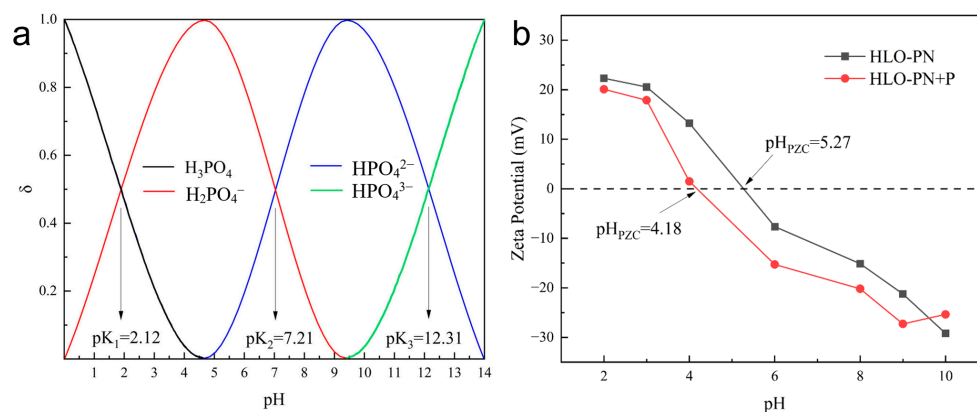
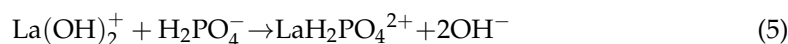
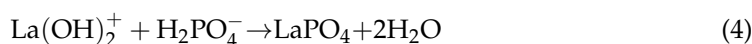
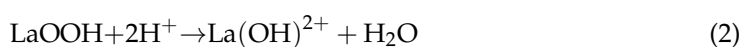
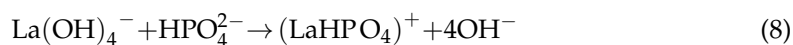
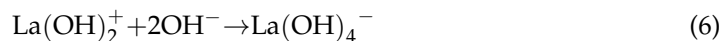


Figure 7. (a) Existence forms of phosphates in different environmental pH levels; (b) zeta potential of HLO-PN before and after phosphate adsorption.

The form in which LaOOH exists changes in solutions of different pH. Under acidic conditions (low pH), LaOOH exists as La^{3+} (Equation (1)). As the pH increases, LaOOH gradually exists in the form of hydroxides such as $\text{La}(\text{OH})_2^{2+}$ and $\text{La}(\text{OH})_2^+$ [45]. Specifically, at low pH of 1.0–3.0, two phosphates exist (i.e., H_3PO_4 and H_2PO_4^-); however, the adsorption of phosphate by HLO-PN is relatively low due to the predominant form of phosphate (H_3PO_4) and the leached form of La (La^{3+}). However, when the pH varies from 3.0 to 5.0, H_2PO_4^- becomes dominant and there is also positively charged HLO-PN ($\text{pH} < \text{pH}_{\text{PZC}} = 5.27$). Therefore, the protonated $\text{La}(\text{OH})_2^+$ and the negatively charged H_2PO_4^- , a combination of electrostatic attraction (Equation (4)) and ligand exchange (Equation (5)), leads to an increase in phosphate removal.

When the solution pH is higher than 5.27, the electrostatic attraction of HLO-PN decreases due to H_2PO_4^- 's reduction of the negatively charged HLO-PN (Equation (6)); the electrostatic attraction decreases accordingly, leading to a decrease in phosphate removal. However, phosphate adsorption remained high and stable between pH 5.3–7.0 due to the $\text{La}(\text{OH})_4^-$ ligand exchange with phosphate ions counteracting the decrease in electrostatic attraction (Equations (7) and (8)). When the solution pH was higher than 7.0, phosphate removal decreased due to the weakening of electrostatic attraction and ligand exchange.





3.3.2. FTIR and XPS Analysis

To further explore the potential functional groups involved in phosphate adsorption, FTIR and XPS analyses were used to characterize the changes in the surface chemistry of HLO-PN before and after adsorption. As shown in Figures 2f and 8a, the peak of HLO-PN+P at 1050 cm^{-1} corresponds to the stretching vibration of P-O [46], indicating that the phosphate has been successfully bound to HLO-PN. In addition, compared with Figure 2f, it was found that the peak intensity of HLO-PN associated with -OH (i.e., 3411 cm^{-1}) decreased after the adsorption of phosphate, suggesting that -OH was involved in the adsorption process of phosphate [26].

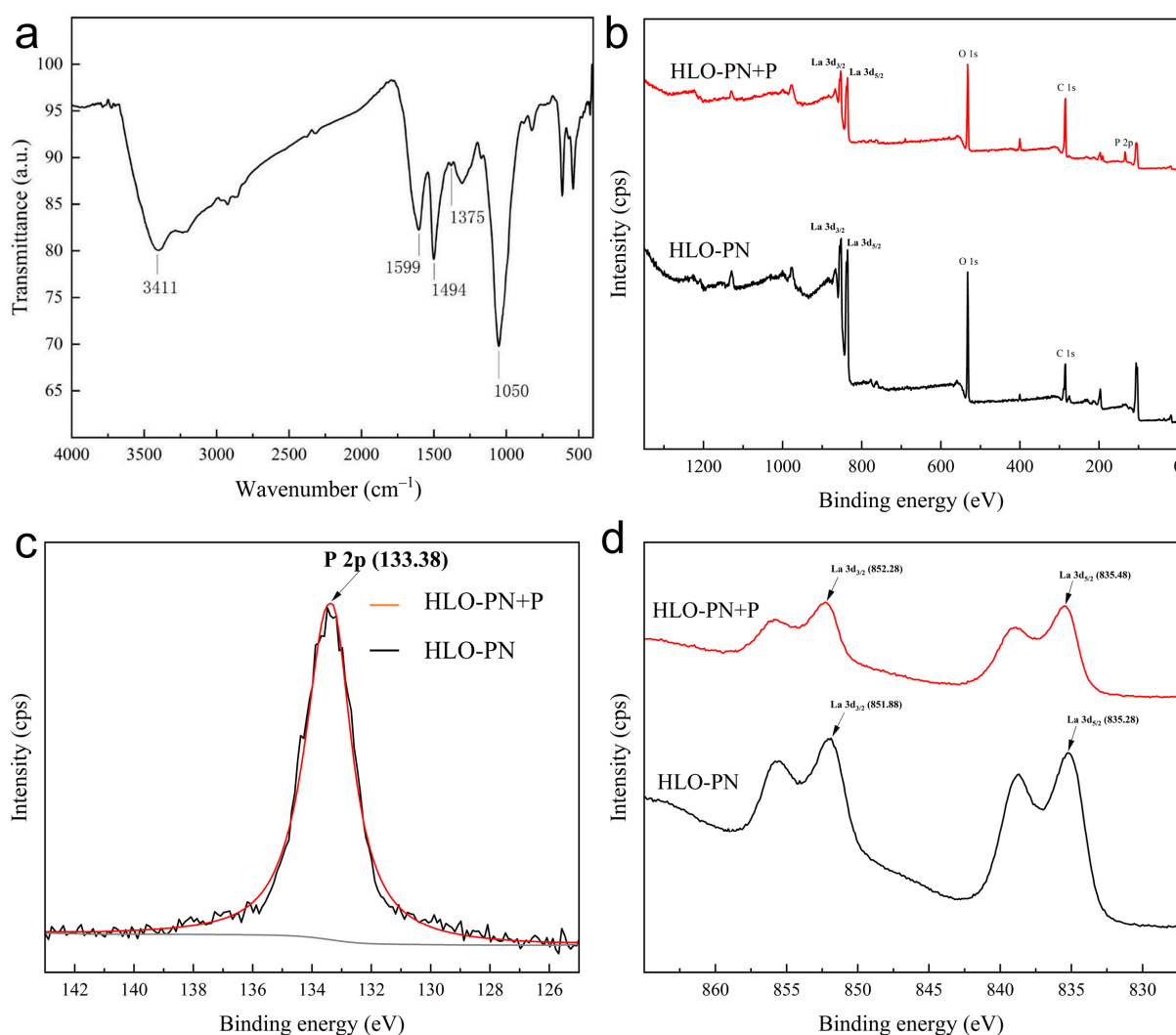


Figure 8. (a) FTIR spectra of HLO-PN after phosphate adsorption. (b) Total survey scans of XPS spectra of HLO-PN before and after phosphate adsorption. (c) High-resolution XPS spectra of P 2p for HLO-PN+P. (d) High-resolution XPS spectra of La 3d for HLO-PN+P.

From the total XPS scan (Figure 8b), it can be seen that there is a unique peak of La 3d in HLO-PN, while a new peak of P 2p appears after adsorption of phosphate, implying that a large amount of phosphate is adsorbed onto HLO-PN. Specifically, as shown in Figure 8c,

the peak detected at 133.38 eV in HLO-PN is attributed to the unique band of P 2p [47]. This band is between 135.20 eV and 132.30 eV and corresponds to HPO_4^{2-} and H_2PO_4^- , indicating that these substances are adsorbed onto HLO-PN [48]. In addition, XPS La 3d high-resolution scans (Figure 8d) showed that the binding energy peaks were 835.28 eV for La $3d_{5/2}$ and 851.88 eV for La $3d_{3/2}$ before the adsorption of phosphate, but these two peaks did not change much after the adsorption of phosphate. This is related to the electronic transition and conformation of La-O-P intra-sphere complexation [49]. Overall, La groups on HLO-PN enhance phosphate adsorption via intra-sphere complexation via ligand exchange.

Taken together, electrostatic attraction and ligand exchange effects were the main mechanisms of phosphate adsorption by HLO-PN (Figure 9).

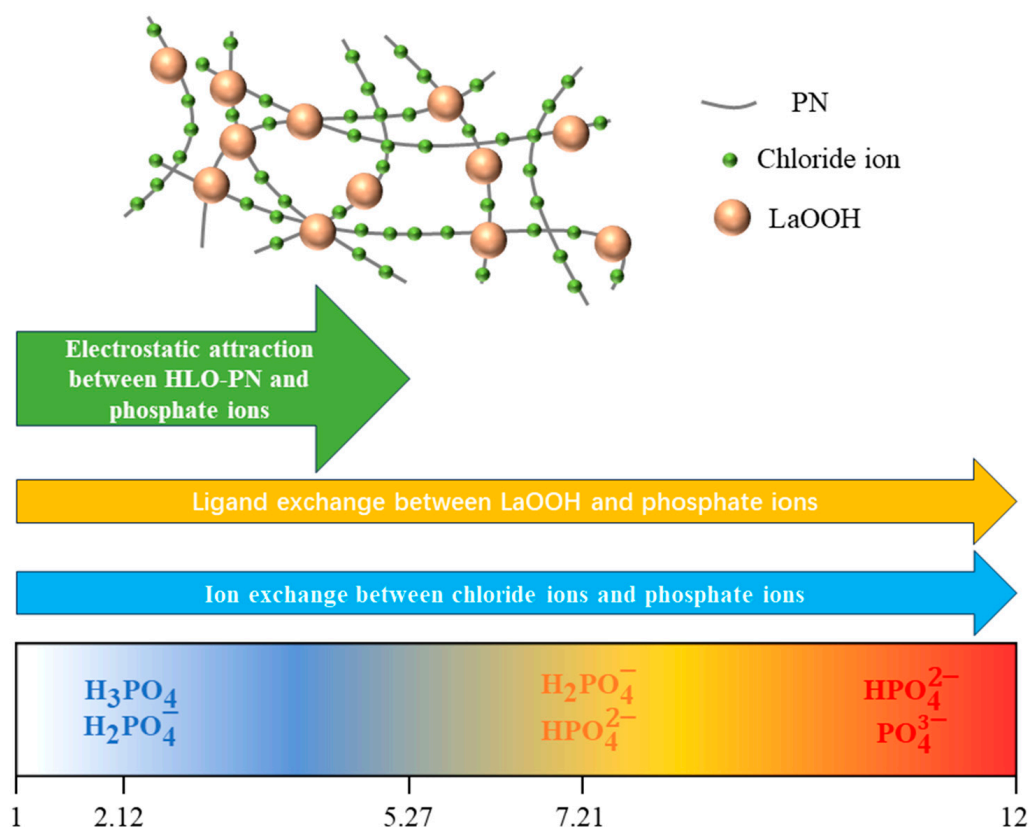


Figure 9. Schematic diagram of phosphate adsorption mechanism by HLO-PN.

3.4. Desorption and Regeneration

Figure S2 depicts the desorption efficiency and the corresponding readsorption capacity for different concentrations of NaOH. The adsorbent for desorption was HLO-PN, saturated at an initial phosphate concentration of 200 mg/L, an initial pH of 5.0, a dosage of 1.5 g/L and a temperature of 25 °C. It was observed that the desorption efficiency increased slightly with increasing NaOH concentration (50 mL), reaching a maximum of 96.29% when the NaOH concentration was 3 M. However, the readsorption capacity of this group was unexpectedly poor, suggesting that high concentrations of NaOH can have an irreversible effect on the adsorbent. At a concentration of 0.5 M NaOH, HLO-PN reached its maximum phosphate readsorption capacity of 75.95 mg/g. For this investigation, a 0.5 M NaOH solution was chosen as the desorbent.

To further investigate the reusability of the regenerated material, five cycles of adsorption and regeneration of HLO-PN were performed. As shown in Figure S3, under the desorption condition of 0.5 M NaOH solution (50 mL), the adsorbed phosphate was recovered in large amounts, and more than 91% of the adsorbed phosphate was still recovered after five consecutive adsorption–desorption cycles. Meanwhile, the regenerated HLO-PN

was effective in phosphate removal, and after five consecutive adsorption–desorption cycles, the phosphate adsorption (60.06 mg/g) was still 74.28% of the initial adsorption (80.85 mg/g). Therefore, after recovering the adsorbed phosphate, the regenerated HLO-PN can be reused for effective phosphate removal from water.

4. Conclusions

A lanthanide-based nanocomposite was developed by introducing hydrated lanthanum oxide (HLO) nanoparticles into quaternized polyaniline (PN) for effective phosphate removal from water. Batch adsorption studies showed that PN exhibited good removal efficiency (>80%) at pH 3.0–5.0; HLO-PN exhibited good removal efficiency in the pH range of 3.0–7.0 and increased the alkalinity of the final solution, which helped to alleviate the problem of acidity in water and was effective against a variety of coexisting ions, such as coexisting anions F^- , Cl^- , NO_3^- and SO_4^{2-} , with good anti-interference ability. In addition, the quasi-secondary kinetic model and Langmuir model had the best fit with experimental data, suggesting that the adsorption process was related to monolayer adsorption with a maximum adsorption of 92.57 mg/g. Further adsorption mechanism studies showed that the adsorption of phosphoric acid on HLO-PN was combined with the inner-sphere complexation by electrostatic attraction and ligand exchange. Finally, the reusability of HLO-PN was verified by the regeneration test, which still recovered more than 91% of the adsorbed phosphate after five consecutive adsorption–desorption cycles, and the regenerated HLO-PN showed good phosphate removal, with the phosphate adsorption still being 74.28% of the initial adsorption after five consecutive adsorption–desorption cycles. Comprehensively, HLO-PN showed excellent phosphate adsorption performance, good regeneration performance and selective adsorption capacity, and can be used as a highly efficient phosphate adsorbent in the field of water treatment.

Supplementary Materials: The following supporting information can be downloaded at <https://www.mdpi.com/article/10.3390/suschem5040017/s1>: Figure S1. Influence of (a) PS, (b) PN and (c) HLO-PN dosage on phosphate removal rate; Figure S2. Effect of NaOH concentration on HLO-PN desorption and readsorption of phosphate; Figure S3. Adsorption capacity and desorption efficiency of HLO-PN for five cycles of adsorption–desorption; Table S1. Specific surface area, porosity and average pore size of the adsorbent; Table S2. Pseudo-first-order and pseudo-second-order kinetic parameters of phosphate adsorption by PN and HLO-PN; Table S3. Kinetic parameters of in-particle diffusion of phosphate adsorbed by PN and HLO-PN; Table S4. Langmuir and Freundlich isotherm parameters of phosphate adsorption by PN and HLO-PN; Table S5. Temkin and D-R isotherm parameters of phosphate adsorption by PN and HLO-PN.

Author Contributions: Conceptualization, M.F. and H.W.; methodology, M.F. and H.W.; validation, M.F. and E.J.; investigation, M.F. and E.J.; writing—original draft preparation, E.J.; writing—review and editing, H.W.; supervision, H.W. All authors have read and agreed to the published version of the manuscript.

Funding: This research received no external funding.

Data Availability Statement: The data presented in this study are available on request from the corresponding author due to privacy.

Conflicts of Interest: Author Minglong Fang has received research grants from Architectural Design and Research Institute Co. Ltd., Nanjing Tech University. The authors declare no conflicts of interest.

References

1. Neal, C.; Jarvie, H.P.; Withers, P.J.A.; Whitton, B.A.; Neal, M. The strategic significance of wastewater sources to pollutant phosphorus levels in English rivers and to environmental management for rural, agricultural and urban catchments. *Sci. Total Environ.* **2010**, *408*, 1485–1500. [[CrossRef](#)] [[PubMed](#)]
2. Nyenje, P.M.; Foppen, J.W.; Uhlenbrook, S.; Kulabako, R.; Muwanga, A. Eutrophication and nutrient release in urban areas of sub-Saharan Africa—A review. *Sci. Total Environ.* **2010**, *408*, 447–455. [[CrossRef](#)] [[PubMed](#)]
3. So, I.; Ogueri, C.; Mno, A. Seasonal variation in physicochemical characteristics of Agulu Lake, South Eastern Nigeria. *Int. J. Fish. Aquat. Stud.* **2021**, *9*, 91–97. [[CrossRef](#)]

4. Mallin, M.A.; Cahoon, L.B. The Hidden Impacts of Phosphorus Pollution to Streams and Rivers. *Bioscience* **2020**, *70*, 315–329. [[CrossRef](#)]
5. De Kock, L.-A. Hybrid Ion Exchanger Supported Metal Hydroxides for the Removal of Phosphate from Wastewater. Ph.D. Thesis, University of Johannesburg, Johannesburg, South Africa, 2015.
6. Li, S.; Zeng, W.; Ren, Z.; Jia, Z.; Wu, G.; Peng, Y. Performance difference of hydrated phosphophilic metal oxides in modifying diatomite and recovering phosphorus from wastewater. *Colloids Surf. A Physicochem. Eng. Asp.* **2021**, *623*, 126763. [[CrossRef](#)]
7. Sun, Y.; Gu, Y.; Xiao, S. Adsorption behaviors and mechanisms of Al-Fe dual-decorated biochar adsorbent for phosphate removal from rural wastewater. *J. Dispers. Sci. Technol.* **2022**, *44*, 2520–2531. [[CrossRef](#)]
8. Wang, X.; Li, Y.; Wen, X.; Liu, L.; Zhang, L.; Long, M. Cooperation of ferrous ions and hydrated ferric oxide for advanced phosphate removal over a wide pH range: Mechanism and kinetics. *Water Res.* **2024**, *249*, 120969. [[CrossRef](#)]
9. Altaf, R.; Sun, B.; Lu, H.J.; Zhao, H.P.; Liu, D.Z. Removal and recovery of phosphonates from wastewater via adsorption. *Crit. Rev. Environ. Sci. Technol.* **2023**, *53*, 1032–1058. [[CrossRef](#)]
10. Boels, L.; Keesman, K.J.; Witkamp, G.J. Adsorption of Phosphonate Antiscalant from Reverse Osmosis Membrane Concentrate onto Granular Ferric Hydroxide. *Environ. Sci. Technol.* **2012**, *46*, 9638–9645. [[CrossRef](#)]
11. Zenobi, M.C.; Rueda, E.H. Adsorption of Me(II), HEDP, and Me(II)-HEDP onto boehmite at nonstoichiometric Me(II)-HEDP concentrations. *Environ. Sci. Technol.* **2006**, *40*, 3254–3259. [[CrossRef](#)]
12. Martínez, R.J.; Farrell, J. Understanding Nitritoltris(methylenephosphonic acid) reactions with ferric hydroxide. *Chemosphere* **2017**, *175*, 490–496. [[CrossRef](#)] [[PubMed](#)]
13. Qiu, H.; Liang, C.; Yu, J.; Zhang, Q.; Song, M.; Chen, F. Preferable phosphate sequestration by nano-La(III) (hydr)oxides modified wheat straw with excellent properties in regeneration. *Chem. Eng. J.* **2017**, *315*, 345–354. [[CrossRef](#)]
14. Sun, J.; Xie, J.; Liu, C. Investigating asymmetric spatial butterfly-shaped steel arch bridges: A case study. *Proc. Inst. Civ. Eng.—Bridge Eng.* **2020**, *174*, 13–27. [[CrossRef](#)]
15. Pan, B.; Wu, J.; Pan, B.; Lv, L.; Zhang, W.; Xiao, L.; Wang, X.; Tao, X.; Zheng, S. Development of polymer-based nanosized hydrated ferric oxides (HFOs) for enhanced phosphate removal from waste effluents. *Water Res.* **2009**, *43*, 4421–4429. [[CrossRef](#)] [[PubMed](#)]
16. Pan, B.; Xu, J.; Wu, B.; Li, Z.; Liu, X. Enhanced Removal of Fluoride by Polystyrene Anion Exchanger Supported Hydrous Zirconium Oxide Nanoparticles. *Environ. Sci. Technol.* **2013**, *47*, 9347–9354. [[CrossRef](#)]
17. Dong, S.; Wang, Y.; Zhao, Y.; Zhou, X.; Zheng, H. La³⁺/La(OH)₃ loaded magnetic cationic hydrogel composites for phosphate removal: Effect of lanthanum species and mechanistic study. *Water Res.* **2017**, *126*, 433–441. [[CrossRef](#)]
18. Hong, X.; Zhu, S.; Xia, M.; Du, P.; Wang, F. Investigation of the efficient adsorption performance and adsorption mechanism of 3D composite structure La nanosphere-coated Mn/Fe layered double hydroxide on phosphate. *J. Colloid Interface Sci.* **2022**, *614*, 478–488. [[CrossRef](#)]
19. Haghseresht, F.; Wang, S.; Do, D.D. A novel lanthanum-modified bentonite, Phoslock, for phosphate removal from wastewaters. *Appl. Clay Sci.* **2009**, *46*, 369–375. [[CrossRef](#)]
20. Chen, N.; Ni, C.; Wu, S.; Chen, D.; Pan, B. Enhanced phosphate removal from water by hydrated neodymium oxide-based nanocomposite: Performance, mechanism, and validation. *J. Colloid Interface Sci.* **2023**, *633*, 866–875. [[CrossRef](#)]
21. Nguyen, T.A.H.; Ngo, H.H.; Guo, W.S.; Zhang, J.; Liang, S.; Lee, D.J.; Nguyen, P.D.; Bui, X.T. Modification of agricultural waste/by-products for enhanced phosphate removal and recovery: Potential and obstacles. *Bioresour. Technol.* **2014**, *169*, 750–762. [[CrossRef](#)]
22. Hong, L.; Wang, W.; Gao, D.; Liu, W. Critical pore size for micropore filling in coal samples with different rank coals. *PLoS ONE* **2022**, *17*, e0264225. [[CrossRef](#)] [[PubMed](#)]
23. Wang, H.; Zhu, A.; Zhu, Z. Preparation of Complex of Polyaniline and Acrylic Ester Grafting Epoxy for Anticorrosion and Intrinsically Antistatic Coatings. In Proceedings of the International Conference on Industrial Application Engineering 2015, Kitakyushu, Fukuoka, Japan, 28–31 March 2015.
24. Gusain, M.; Nagarajan, R.; Singh, S.K. Highly ordered polyaniline: Synthesis, characterization and electrochemical properties. *Polym. Bull.* **2020**, *77*, 3277–3286. [[CrossRef](#)]
25. Hammadi, A.H.; Assi, L.N.; Hussien, F.H.; Hussien, F.H. Drug Loading on Carbon Nanotubes synthesized by Flame Fragments Deposition Technique. *Syst. Rev. Pharm.* **2020**, *11*, 275–281. [[CrossRef](#)]
26. Sonwani, R.; Gupta, S.; Soni, R. Production of bioethanol from biodegraded alkali pretreated rice straw. *Vegetos* **2020**, *33*, 128–134. [[CrossRef](#)]
27. Irshad, K.; Anees, P.; Rajitha, R.; Ravindran, T.; Srihari, V.; Kalavathi, S.; Shekar, N.C. Anomalous lattice compression in the hexagonal La₂O₃—A high pressure X-ray diffraction, Raman spectroscopy and first principle study. *J. Alloys Compd.* **2020**, *822*, 153657. [[CrossRef](#)]
28. Wang, N.; Feng, J.T.; Chen, J.; Wang, J.N.; Yan, W. Adsorption mechanism of phosphate by polyaniline/TiO₂ composite from wastewater. *Chem. Eng. J.* **2017**, *316*, 33–40. [[CrossRef](#)]
29. Revellame, E.D.; Fortela, D.L.; Sharp, W.; Hernandez, R.; Zappi, M.E. Adsorption kinetic modeling using pseudo-first order and pseudo-second order rate laws: A review. *Clean. Eng. Technol.* **2020**, *1*, 100032. [[CrossRef](#)]
30. Wang, J.; Guo, X. Rethinking of the intraparticle diffusion adsorption kinetics model: Interpretation, solving methods and applications. *Chemosphere* **2022**, *309*, 136732. [[CrossRef](#)]

31. Biswas, S.; Mohapatra, S.S.; Kumari, U.; Meikap, B.C.; Sen, T.K. Batch and continuous closed circuit semi-fluidized bed operation: Removal of MB dye using sugarcane bagasse biochar and alginate composite adsorbents. *J. Environ. Chem. Eng.* **2020**, *8*, 103637. [[CrossRef](#)]
32. Kalam, S.; Abu-Khamsin, S.A.; Kamal, M.S.; Patil, S. Surfactant adsorption isotherms: A review. *ACS Omega* **2021**, *6*, 32342–32348. [[CrossRef](#)]
33. Kilic, G.; Ilik, E.; Mahmoud, K.; El-Mallawany, R.; El-Agawany, F.; Rammah, Y. Novel zinc vanadyl boro-phosphate glasses: ZnO–V₂O₅–P₂O₅–B₂O₃: Physical, thermal, and nuclear radiation shielding properties. *Ceram. Int.* **2020**, *46*, 19318–19327. [[CrossRef](#)]
34. Kiran, B.; Kaushik, A. Chromium binding capacity of *Lyngbya putealis* exopolysaccharides. *Biochem. Eng. J.* **2008**, *38*, 47–54. [[CrossRef](#)]
35. Hu, X.-J.; Wang, J.-S.; Liu, Y.-G.; Li, X.; Zeng, G.-M.; Bao, Z.-L.; Zeng, X.-X.; Chen, A.-W.; Long, F. Adsorption of chromium (VI) by ethylenediamine-modified cross-linked magnetic chitosan resin: Isotherms, kinetics and thermodynamics. *J. Hazard. Mater.* **2011**, *185*, 306–314. [[CrossRef](#)] [[PubMed](#)]
36. Lu, H.; Yang, L.; Shabbir, S.; Wu, Y. The adsorption process during inorganic phosphorus removal by cultured periphyton. *Environ. Sci. Pollut. Res.* **2014**, *21*, 8782–8791. [[CrossRef](#)]
37. Fang, L.; Liu, R.; Li, J.; Xu, C.; Huang, L.-Z.; Wang, D. Magnetite/Lanthanum hydroxide for phosphate sequestration and recovery from lake and the attenuation effects of sediment particles. *Water Res.* **2018**, *130*, 243–254. [[CrossRef](#)]
38. Wang, Y.Y.; Yang, X.Y.; Dai, J.D.; Yan, Y.S.; Jiang, Y.H.; Chen, L. 3D lanthanum modified cellulose aerogel based on filter paper with excellent adsorption performance for phosphate. *Cellulose* **2023**, *30*, 10413–10426. [[CrossRef](#)]
39. Wu, Y.; Li, X.; Yang, Q.; Wang, D.; Xu, Q.; Yao, F.; Chen, F.; Tao, Z.; Huang, X. Hydrated lanthanum oxide-modified diatomite as highly efficient adsorbent for low-concentration phosphate removal from secondary effluents. *J. Environ. Manag.* **2019**, *231*, 370–379. [[CrossRef](#)]
40. Xie, J.; Wang, Z.; Fang, D.; Li, C.J.; Wu, D.Y. Green synthesis of a novel hybrid sorbent of zeolite/lanthanum hydroxide and its application in the removal and recovery of phosphate from water. *J. Colloid Interface Sci.* **2014**, *423*, 13–19. [[CrossRef](#)]
41. Karthikeyan, P.; Banu, H.A.T.; Meenakshi, S. Removal of phosphate and nitrate ions from aqueous solution using La³⁺ incorporated chitosan biopolymeric matrix membrane. *Int. J. Biol. Macromol.* **2019**, *124*, 492–504. [[CrossRef](#)]
42. Huang, W.Y.; Li, D.; Liu, Z.Q.; Tao, Q.; Zhu, Y.; Yang, J.; Zhang, Y.M. Kinetics, isotherm, thermodynamic, and adsorption mechanism studies of La(OH)₃-modified exfoliated vermiculites as highly efficient phosphate adsorbents. *Chem. Eng. J.* **2014**, *236*, 191–201. [[CrossRef](#)]
43. Zhang, S.; Lin, T.; Li, W.; Li, M.; Su, K.; Chen, J.; Yang, H. Lanthanum-loaded peanut shell biochar prepared via one-step pyrolysis method for phosphorus removal and immobilization. *Environ. Technol.* **2023**, *44*, 1169–1178. [[CrossRef](#)] [[PubMed](#)]
44. García, K.I.; Quezada, G.R.; Arumi, J.L.; Urrutia, R.; Toledo, P.G. Adsorption of phosphate ions on the basal and edge surfaces of kaolinite in low salt aqueous solutions using molecular dynamics simulations. *J. Phys. Chem. C* **2021**, *125*, 21179–21190. [[CrossRef](#)]
45. Schüßler, F.; Pidko, E.A.; Kolvenbach, R.; Sievers, C.; Hensen, E.J.; van Santen, R.A.; Lercher, J.A. Nature and location of cationic lanthanum species in high alumina containing faujasite type zeolites. *J. Phys. Chem. C* **2011**, *115*, 21763–21776. [[CrossRef](#)]
46. Zhou, Z.; Wang, E.; Liang, Y.; Miao, Y.; Chen, H.; Ling, M.; Li, W.; Huang, J.; Zhang, W. Bio-based PA-grafted bamboo charcoal for improving the flame retardancy of PLA/PCL film without damaging mechanical properties and degradability. *Ind. Crops Prod.* **2024**, *210*, 118182. [[CrossRef](#)]
47. Sun, B.; Ni, J. Self-supported TiO₂@P nanotube arrays as high-performance anodes for sodium-ion batteries. *Funct. Mater. Lett.* **2022**, *15*, 2250019. [[CrossRef](#)]
48. Zhang, Y.; Akindolie, M.S.; Tian, X.; Wu, B.; Hu, Q.; Jiang, Z.; Wang, L.; Tao, Y.; Cao, B.; Qu, J. Enhanced phosphate scavenging with effective recovery by magnetic porous biochar supported La(OH)₃: Kinetics, isotherms, mechanisms and applications for water and real wastewater. *Bioresour. Technol.* **2021**, *319*, 124232. [[CrossRef](#)]
49. Zhang, P.; He, M.; Xu, Z.; Li, F.; Fang, D.; Li, C.; Lv, C.; Mo, X.; Li, K.; Wang, H. Incorporation of edge-N into La-doped hierarchical carbon framework enables high-efficiency phosphate electroadsorption: Boosting accessible active centers and bridging charge transfer paths. *Chem. Eng. J.* **2024**, *481*, 148518. [[CrossRef](#)]

Disclaimer/Publisher’s Note: The statements, opinions and data contained in all publications are solely those of the individual author(s) and contributor(s) and not of MDPI and/or the editor(s). MDPI and/or the editor(s) disclaim responsibility for any injury to people or property resulting from any ideas, methods, instructions or products referred to in the content.